The Hot Deformation Behavior of an As-Cast Alloy 718 Ingot

M.J. Weis*, M.C. Mataya*, S.W. Thompson, and D.K. Matlock

Advanced Steel Processing and Products Research Center
Colorado School of Mines
Golden, Colorado

*Rockwell International Corporation
Golden, Colorado

ABSTRACT

The hot deformation characteristics of an as-cast 406mm diameter vacuum induction melted-vacuum arc remelted alloy 718 ingot were investigated as a function of strain, strain rate, and temperature with high temperature compression tests between 950°C and 1150°C. The compression data exhibited a peak in the flow stress followed by extensive strain softening at low temperatures and esentially constant flow stresses at high temperatures. The observed transition in deformation behavior was attributed to the effects of temperature on strain softening mechanisms, primarily dynamic recovery, adiabatic heating and its effects on dynamic recovery, and shear band formation. The data suggest that hot working in the temperature range of 1050-1150°C will enhance uniform breakdown through larger sections. Microstructural analysis with both light and electron microscopy, showed that limited dynamic recrystallization occurred. The results are analyzed to identify mechanisms for microstructural refinement in cast ingots.

Superalloy 718—Metallurgy and Applications
Edited by E.A. Loria
The Minerals, Metals & Materials Society, 1989

INTRODUCTION

The need for uniform microstructures and properties in industrial parts requires that careful consideration be given to the choice of the mechanical hot deformation techniques which are utilized during all stages of processing. During ingot breakdown by either rolling or forging, the primary processor must use reduction schedules which are both economical and attempt to transform the inhomogeneous cast ingot structure into a uniform structure. Subsequent working during final processing can also further homogenize the microstructure.

Despite the fact that processing procedures from the cast ingot to the final part all have an impact on final material structure and properties, most of the development work to understand and improve properties and structure has focused on the final processing stage [1-11]. In contrast, limited studies have considered the development of structure and properties from the initial cast ingot [12-14].

In general, due to the size of material being formed, deformation requirements during primary breakdown are significantly different than for final component fabrication. For example, average strains imposed in each deformation cycle during breakdown of large ingots are typically low and non-uniform and result in non-uniform recrystallized microstructures. During working, as the size of the worked product decreases, the potential for imposing higher and more uniform strain fields, which correspondingly produce more uniform recrystallized microstructures, increases.

To provide an improved understanding of microstructural development in hot formed alloy 718, this study was undertaken to evaluate the effects of strain, strain rate, and temperature on microstructural evolution during primary breakdown of an as-cast alloy 718 ingot. This study is an extension of a previous study [15,16] and is directly related to the work of Mataya and Matlock in this publication [17].

EXPERIMENTAL PROCEDURE

A section of a 406mm diameter as-cast vacuum induction melted ingot of alloy 718 was received from the Carpenter Technology Corporation for analysis and a complete discussion of the processing history of the ingot is included elsewhere [16]. The ingot was sectioned in both the longitudinal and transverse directions, and the sections were ground and macroetched. The resulting macroetched samples are shown in Fig. 1. While the transverse section (Fig. 1a) shows a relatively uniform structure, the longitudinal section (Fig. 1b) shows that the grain structure varies significantly with radial position and is not symmetric. The grain structure can be viewed as composed of three microstructural zones [15,16,18]: large, pancake-shaped grains near the surface; fine, columnar grains at intermediate radial positions (i.e. starting at about 40mm in from the surface); and a significant core region consisting of large columnar grains. In this study the deformation behavior of the fine columnar grain region is considered; the effect of radial position on properties was considered in a companion study [18]. The composition in wt. pct. is: 18.35Fe, 0.028C, 0.09Mn, 0.11Si, 0.006P, 0.001S, 18.36Cr, 3.12Mo, 0.03Cu, 0.30Co, 0.98Ti, 0.59Al, 0.004B, <0.01Ta, 5.38Nb, and 52.43Ni.

Cylindrical compression samples, 19mm high by 12.7mm in diameter, were machined with the compression axis parallel to the ingot axis from a constant radial position which corresponded to the fine columnar grain

zone identified in Fig. 1. The specimen ends were recessed to constrain the high temperature lubricant. Hot compression tests were performed in air at constant true strain rates on a computer controlled 250kN capacity servo-hydraulic test machine equipped with a high temperature furnance and high temperature compression platens [15,16]. Test specimens were heated for 10 min. in the test system prior to loading. The microstructures of the deformed samples were analyzed using standard light and transmission electron microscopy (TEM) techniques on samples quenched to room temperature immediately after testing (i.e. within 2s) or after a holding period at temperature after testing. The TEM samples were mechanically cut and ground to thicknesses of 0.06 to 0.14 mm. Specimens were jet polished in a solution of 70% ethyl alcohol, 12.5% distilled water, 10% 2-butoxyethanol, and 7.5% perchloric acid at -30°C , 25V, and 55mA.

RESULTS AND DISCUSSION

Hot Compression Data

Hot compression true stress-strain data obtained at 950, 1050, and 1150°C are shown in Figs. 2 - 4, respectively. In each figure data are presented for three true strain rates. Dotted lines on the stress-strain curves indicate that computer generated data were supplemented with points taken from load-displacement curves which were also recorded for each test.

The stress-strain curves in Figs. 2 - 4 indicate that the deformation characteristics of alloy 718 change significantly with strain rate and temperature. At 1150°C (Fig. 2) the samples deformed to a maximum flow stress, and then exhibited a slight decrease in flow stress to a relatively constant value at high strains. These samples also exhibited a small yield point at low strains.

At 1050°C (Fig. 3) the deformation behavior depends on strain rate. For imposed strain rates of 0.01 and 0.1 s^{-1}, the stress-strain curves resemble the curves at 1150°C. However, at a strain rate of 1.0 s^{-1} no yield point was observed, and the sample strain hardened to a peak flow stress at a strain of -0.1. After the peak in flow stress, significant strain softening was observed up to a strain of approximately -0.7.

The stress-strain curves for samples deformed at 950°C exhibited a constant flow stress and a yield point at the lowest strain rate. With an increase in strain rate, the yield point disappeared and the degree of strain softening after the peak stress increased. The presence of the yield drop at high temperatures and low strain rates and the disappearance of the yield drop with decreasing temperature and increasing strain rate agrees with previous work performed on alloy 718 [19,20]. These studies attributed the development of the yield point to precipitates or carbides on dislocations or stacking faults as well as to short range ordering.

The temperature dependent peak flow stress data for each strain rate are summarized in Fig. 5. The maximum flow stress decreased with an increase in temperature and decrease in strain rate, and the magnitudes of the observed flow stresses agree with previous work on wrought samples of the same alloy [20].

The peak flow stress-temperature data were analyzed further to determine the temperature dependence of the strain rate sensitivity, m, as defined by

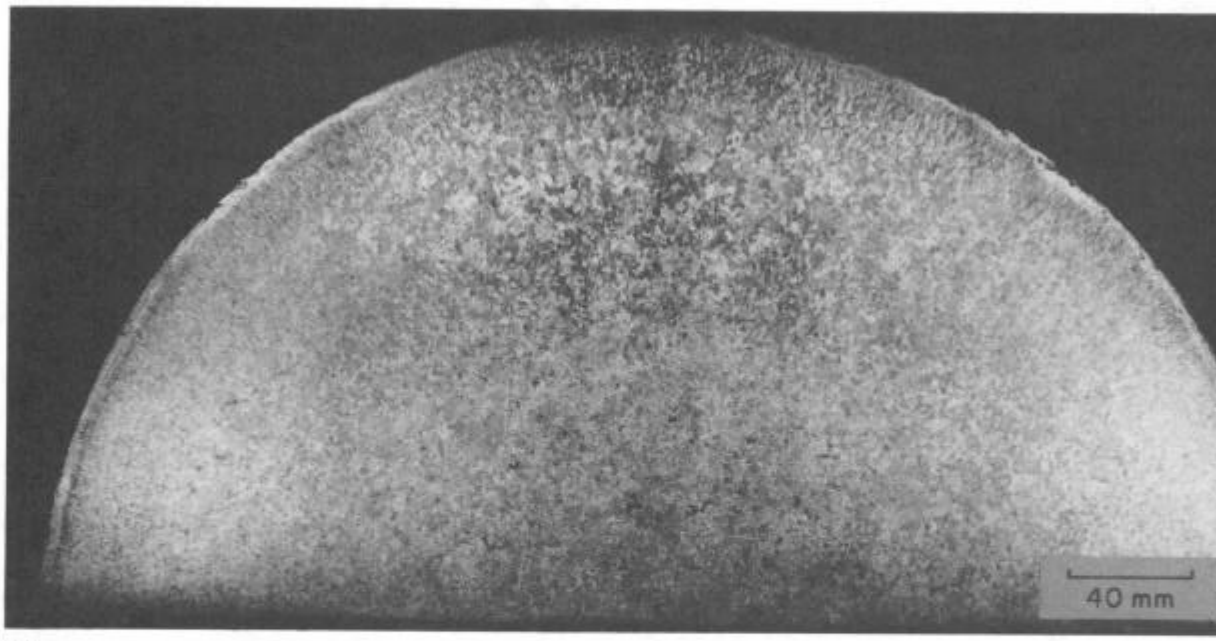

(a)

Figure 1 - Macroetched sections of as-cast alloy 718 ingot (a) transverse, (b) longitudinal. Etched in boiling HCL:HNO_3 at 5:1.

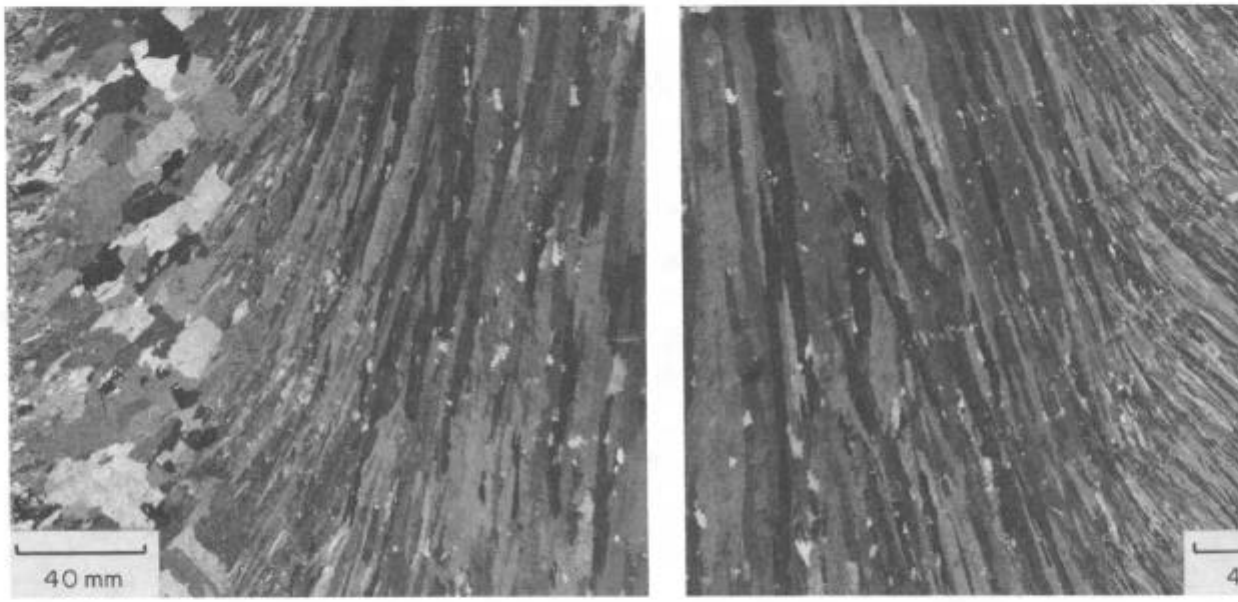

(b)

Figure 1 - (continued)

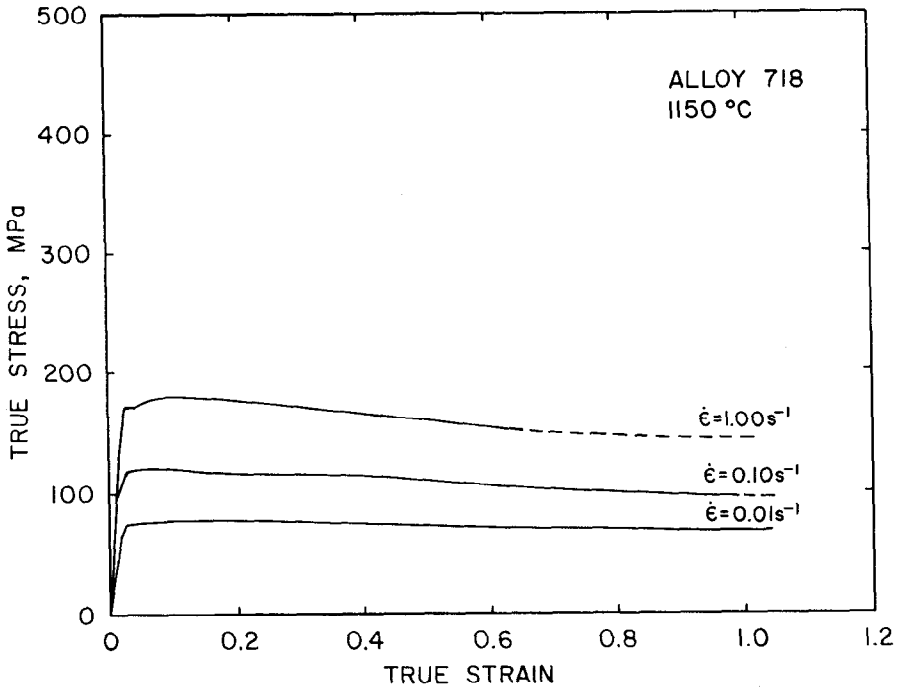

Figure 2 - True stress-true strain compression flow curves for alloy 718 deformed at 1150°C for three true strain rates.

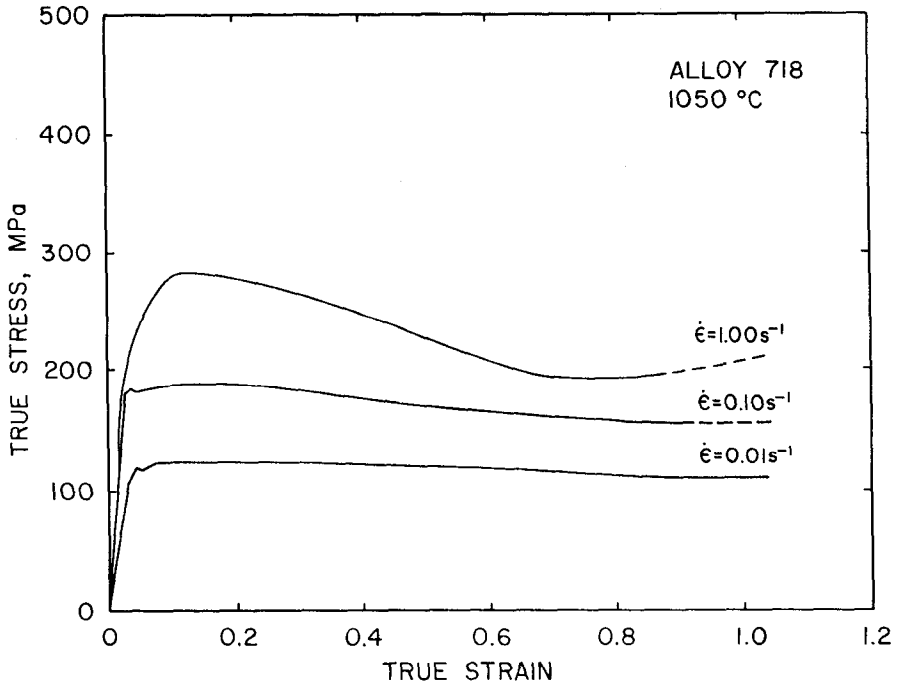

Figure 3 - True stress-true strain compression flow curves for alloy 718 deformed at 1050°C for three true strain rates.

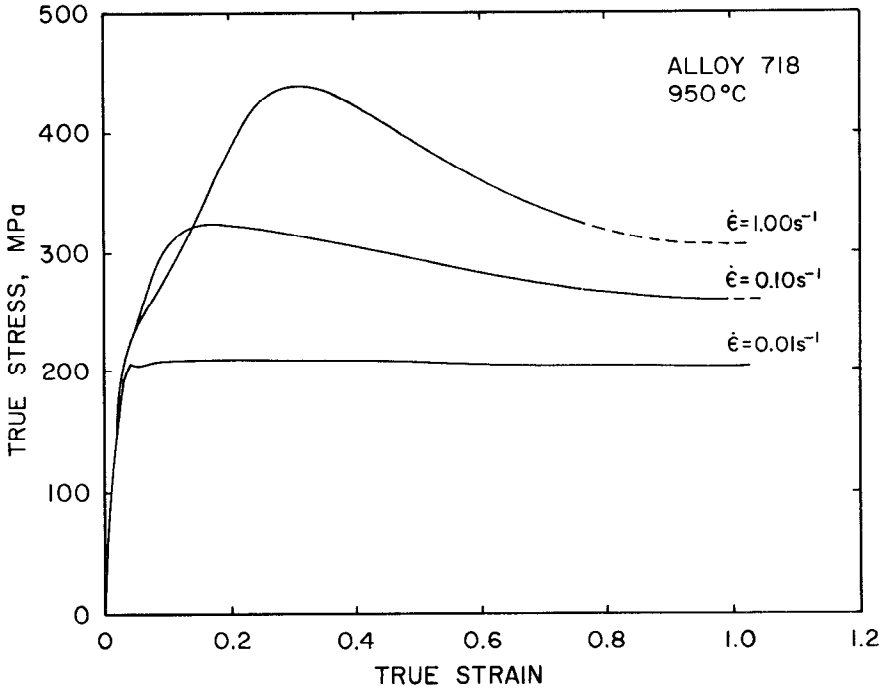

Figure 4 - True stress-true strain compression flow curves for alloy 718 deformed at 950°C for three true strain rates.

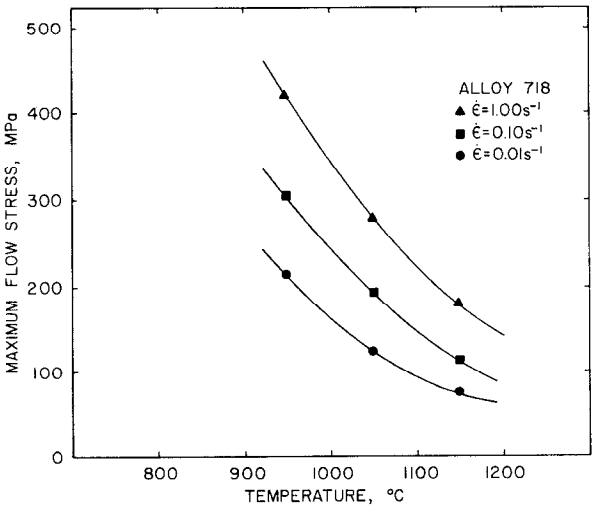

Figure 5 - The effect of test temperature on the peak flow stress in as-cast alloy 718 deformed at three strain rates.

$$\sigma_F = B(\dot{\epsilon})^m \quad (1)$$

where σ_F is the true flow stress at a constant strain and temperature, $\dot{\epsilon}$ is the true strain rate, and B is a constant. The resulting m values for strain rate pairs of 0.01 to 0.1 s^{-1}, m(L), and for strain rate pairs of 0.1 to 1.0 s^{-1}, m(H), at a true strain of -0.6, are shown in Fig. 6. In Fig. 6 T_m is the melting point, taken here as the liquidus, 1260°C. The strain rate sensitivity increased with an increase in temperature and a decrease in imposed strain rate range. These trends are consistent with data for materials which exhibit thermally activated recovery dominated flow.

The combined effects of stress, strain rate, and temperature on the peak flow stress were analyzed with the following constitutive equation approach commonly applied to hot working data. The stress and temperature dependence of the strain rate can be given, in general, by equations of the form:

$$\dot{\epsilon} = Af(\sigma)g(T) \quad (2)$$

where A is a structure dependent constant and the functions f and g may have several forms. Typically, g(T) is given by:

$$g(T) = \exp(-Q/RT) \quad (3)$$

where Q is the apparent activation energy for the deformation process and R and T have their usual meaning. $f(\sigma)$ varies with stress; at low stresses

$$f(\sigma) = \sigma^n \quad (4)$$

and at high stresses

$$f(\sigma) = \exp(\beta\sigma) \quad (5)$$

In Eqs. 4 and 5 n and b are temperature independent constants.

To obtain an activation energy for the high temperature deformation behavior of alloy 718, the following procedure was used to determine constant stress strain rate-temperature pairs. From Fig. 5 temperatures, which correspond to a constant flow stress for each imposed strain rate, were interpolated for a set of arbitrarily chosen stresses. The resulting strain rate-temperature pairs for each stress are plotted according to Eqs. 2 and 3 in Fig. 7 (which also identifies the stresses chosen for the interpolation process). The slopes of all of the lines in Fig. 7 are similar and yield an activation energy of 423 kJ/mole, a value which is in the range of Q values reported for nickel base superalloys [20,21].

To illustrate that a Q of 423 kJ/mole adequately describes the peak flow stress data, all of the peak flow stress data were reevaluated with the following analysis. Combining and rearranging Eqs. 2, 3, and 4 gives the following expression:

$$\sigma = (1/A)\,(\dot{\epsilon} \exp Q/RT)^{1/n} \quad (6)$$

If Eq. 6 adequately describes the data, then a plot of peak stress versus the quantity, $\dot{\epsilon}\exp Q/RT$ (an expression often referred to as the Zener-Hollomon parameter), should produce a single line. This type of plot is presented in Fig. 8. The straight line relationship shows that a

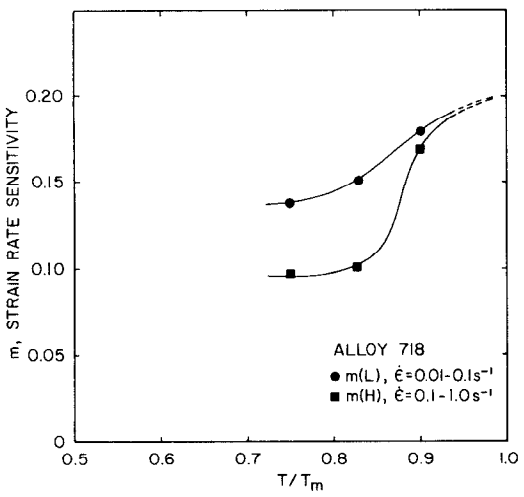

Figure 6 - The dependence of strain rate sensitivity, m evaluated at a true strain of -0.6, on homologous temperature for two strain rate pairs.

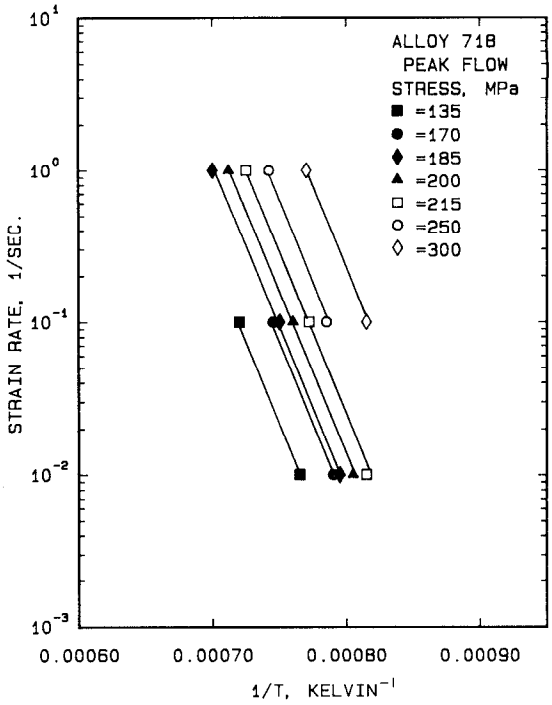

Figure 7 - Strain rate as a function of inverse test temperature for as-cast alloy 718.

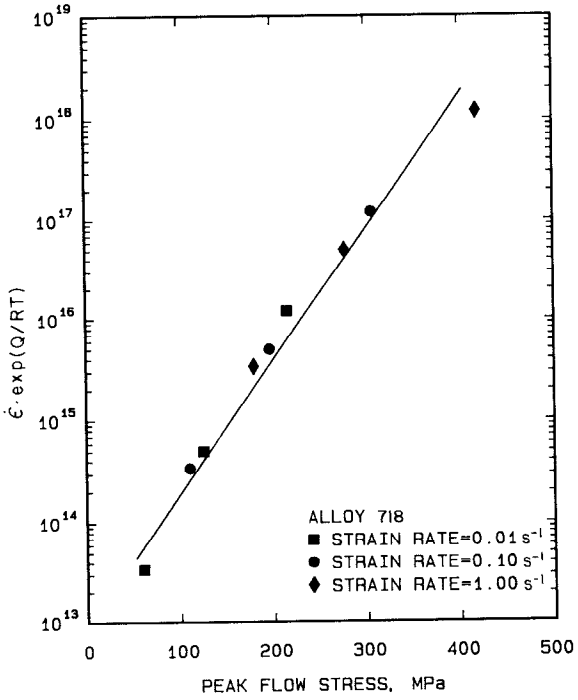

Figure 8 - A correlation of peak flow stress with temperature compensated strain rate plotted according to Eq. (6).

unified equation of the form given in Eq. 6 describes the stress, strain rate, and temperature behavior of as-cast alloy 718.

Microstructural Analysis

Microstructural development, during deformation and as a result of hold time after deformation, was evaluated with light and transmission electron microscopy. Light microscopy of samples which were quenched immediately after deformation (i.e. within 2 s) revealed the existence of several unique features which are illustrated in the series of micrographs included in Figs. 9 and 10. Microstructural features include: development of serrated grain boundaries, Fig. 9a; recrystallization along high angle grain boundaries, Fig. 9b; recrystallization around primary particles, Fig. 9c; annealing or growth twins in recrystallized grains, Fig. 9d; and subtle changes in surface topography within grains giving a general morphology consistent with a dislocation substructure, Fig. 10. These micrographs indicate that recrystallization initiated during deformation but that the bulk of the microstructure was unrecrystallized. Therefore, dynamic recrystallization was not significant during hot deformation of as-cast alloy 718.

The static recrystallization behavior was evaluated with a series of samples which were held at the test temperature for various times after deformation and prior to quenching to room temperature. The effect of hold time is illustrated in Fig. 11 by the series of micrographs for samples deformed at 1150°C to a strain of -0.25 at a strain rate of 1.0 s^{-1}. Recrystallization initiated on high angle grain boundaries (Fig. 11a) and continued around primary particles (Figs. 11b and 11c) until the sample was completely recrystallized (Fig. 11d).

The microstructures of all of the samples included in the hold time study were analyzed to determine the volume percent which was recrystallized and the average recrystallized grain diameter, and the results as a function of hold time are presented in Figs. 12 and 13, respectively. Due to the inhomogeneous microstructure after deformation, the volume percent recrystallized measurements are best estimates from representative micrographs. At 1150°C all samples exhibited standard recrystallization curves and complete recrystallization within 10 minutes. The rate of recrystallization increased with an increase in imposed strain but was essentially independent of the imposed strain rate. In contrast, at 950°C only limited recrystallization occurred.

The average grain size within the recrystallized zones increased with an increase in hold time. After 10 min. at 1150°C the grain size of the fully recrystallized samples was approximately 300 μm. This grain size represents a 10:1 reduction in comparison to the starting structure [16].

Verification that limited dynamic recrystallization occurred was obtained with analysis of detailed transmission electron micrographs, presented in Figs. 14 and 15, of samples deformed at 1150°C at a strain rate of 1.0s^{-1}. Figure 14 shows a sample which was held for 2.5 min. at temperature after deformation to a strain of -0.25. Figures 14a and 14b are micrographs from the same region of a sample and the two X's indicate points which were separated by a distance of approximately 5 μm. Three distinctly different regions are evident. Region A is an unrecrystallized grain, whereas regions B and C are recrystallized. Unrecrystallized regions displayed dislocation tangles and limited evidence for recovery (point a in Fig. 14a). Recrystallized grains also contained a significant number of dislocations, but these arrays were well organized (e.g., point b

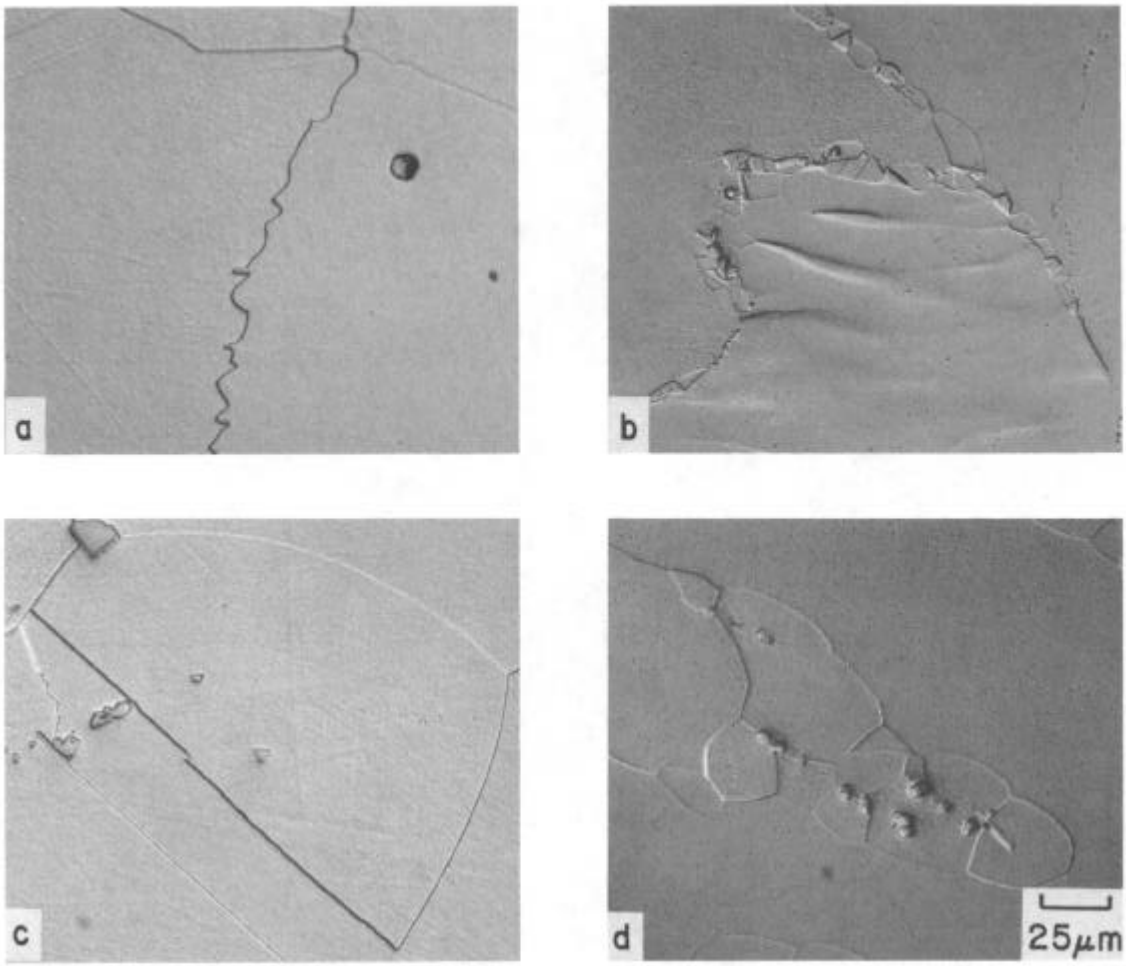

Figure 9 - Selected examples of microstructural features observed after deformation of as-cast alloy 718. (a) serrated grain boundary, (b) recrystallization along high angle grain boundary, (d) recrystallization around primary intermetallic particles, (c) annealing or growth twins in recrystallized grains.

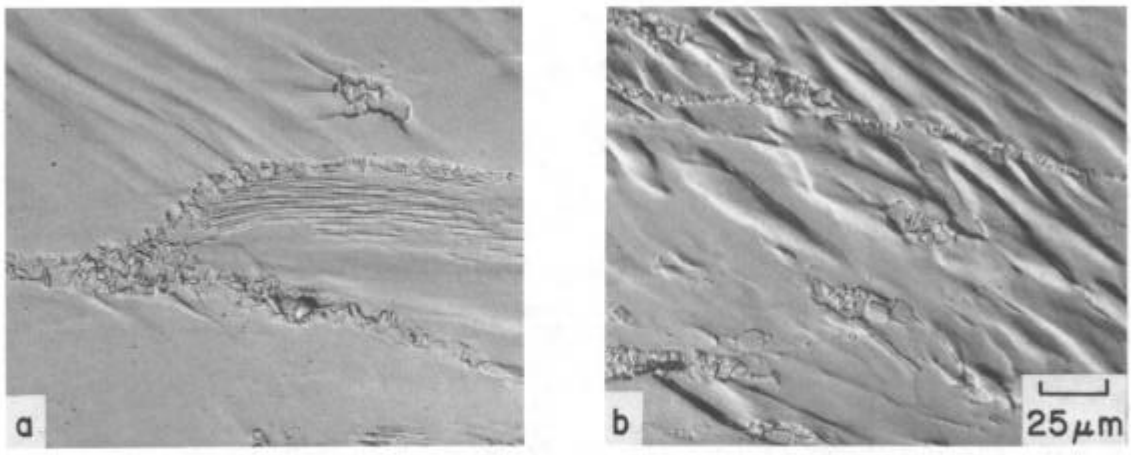

Figure 10 - Selected examples of microstructural features observed after hot deformation of as-cast alloy 718. (a) and (b) surface relief within grains illustrating dislocation substructure development.

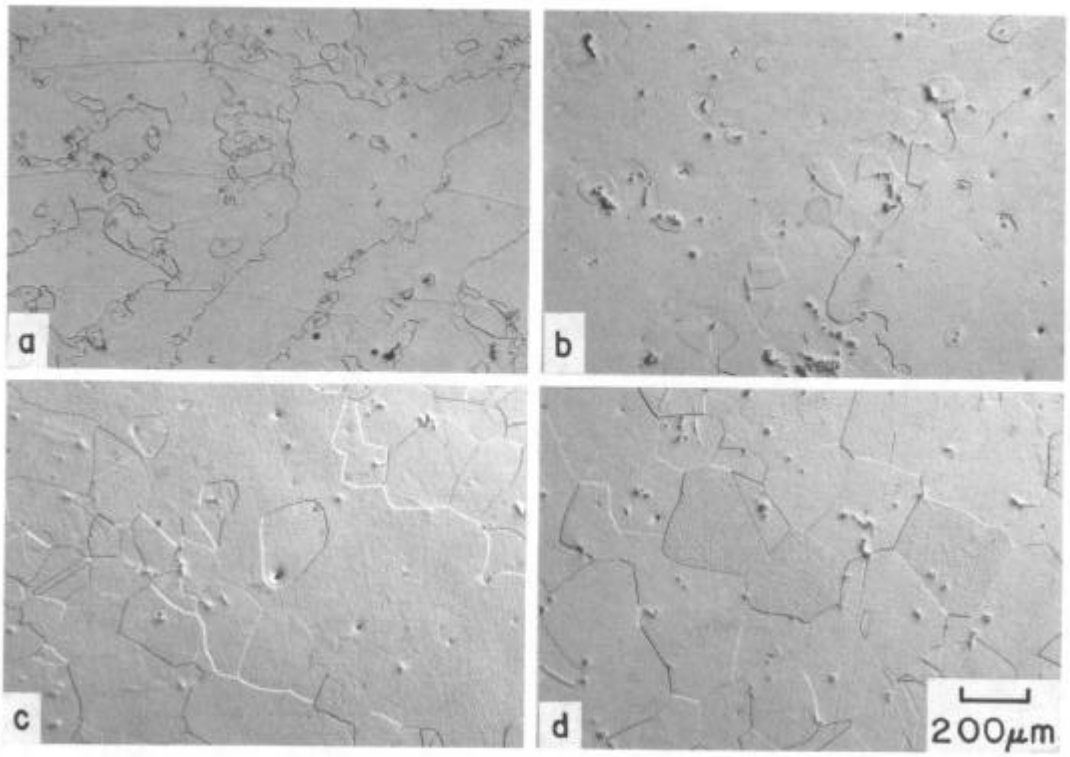

Figure 11 - Light micrographs of samples held at 1150°C after deformation at 1.0 s^{-1} to a strain of -0.25. (a) 1.9s, (b) 38s, (c) 150s, and (d) 600s.

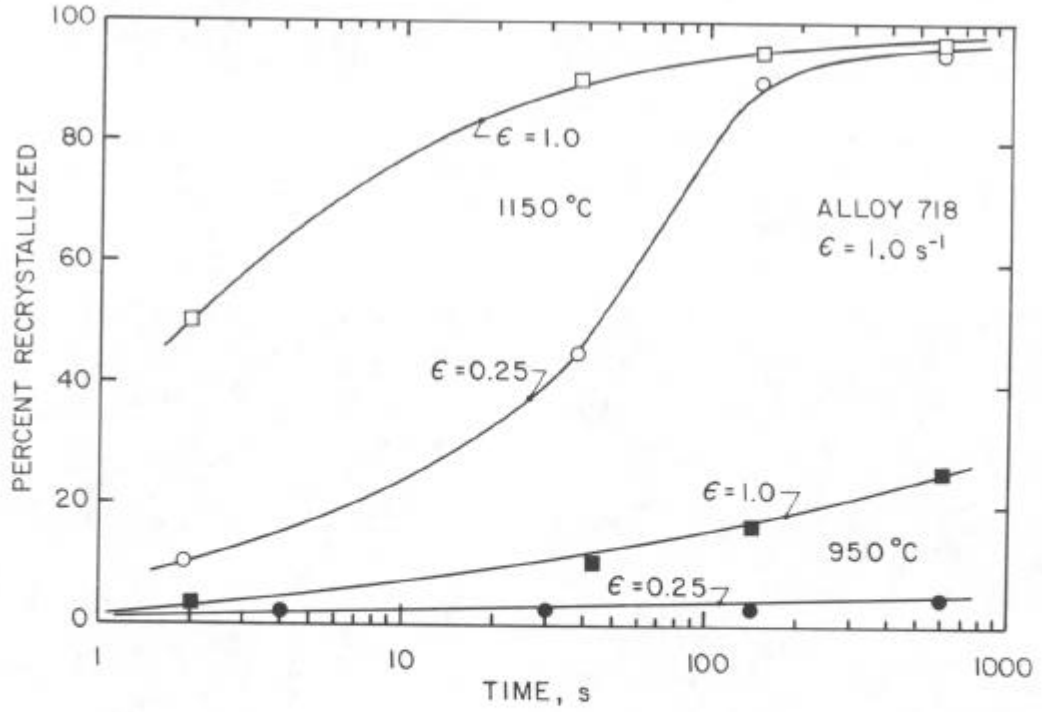

Figure 12 - The effect of hold time after deformation on the percentage of the microstructure which recrystallized at the indicated temperatures. Samples of alloy 718 deformed at a true strain rate of 1.0 s^{-1} to strains of either 0.25 or 1.0.

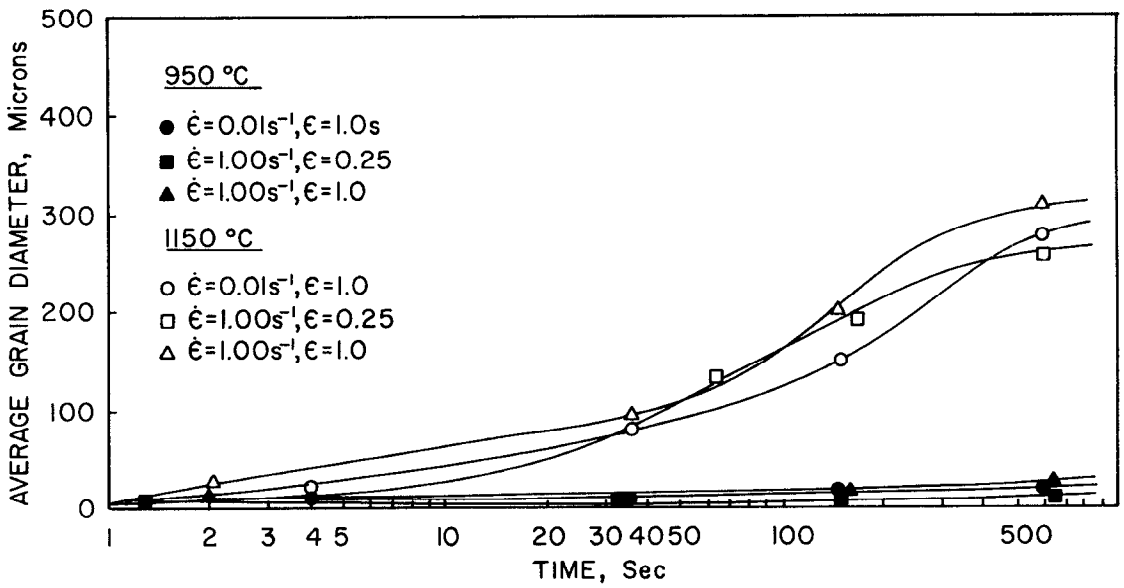

Figure 13 - The effect of hold time after deformation of alloy 718 on the average grain size, measured within the recrystallized regions.

in Fig. 14b), i.e. the dislocations did not deviate from a single slip plane. The presence of these dislocations is unexpected as they are not representative of high temperature deformation structures and are interpreted to result from the effects of residual stresses induced during quenching.

Figure 15 shows a sample which was quenched immediately after deformation to a strain of -1.0. This figure includes both recrystallized grains (identified as A through C) and unrecrystallized regions (grain D). In comparison to Fig. 14, the sample strained to the higher strain exhibits grains with dislocation tangles (i.e. at point a) in addition to extensive evidence for recovery in the form of well-developed low-angle subboundaries. The misorientation across these boundaries was approximatley 1° to 2°. Limited evidence for pinning of migrating subboundaries by unidentified small precipitates was also found (e.g. at point b). Analysis of Fig. 15 indicates that dynamic recrystallization was unlikely and that the primary recrystallization reaction is either static or metadynamic at the high strain level. If a static mechanism is postulated, then it must have occurred in the few seconds required to transfer the sample from the compression system to the quench bath. For both strain levels, linear dislocation arrays were also found in the unrecrystallized regions, but they tended to be less noticeable because of the overall higher dislocation density of these regions.

Analysis of Strain Softening

Strain softening, i.e. the decrease in stress with strain shown in Figs. 2 - 4, is often associated with dynamic recrystallization [5,13,21]. However, based on the microstructural analysis considered above, the observed softening in the cast ingots was due to processes other than dynamic recrystallization. Possible softening mechanisms include the formation of macroscopic shear bands [22] which were observed on the

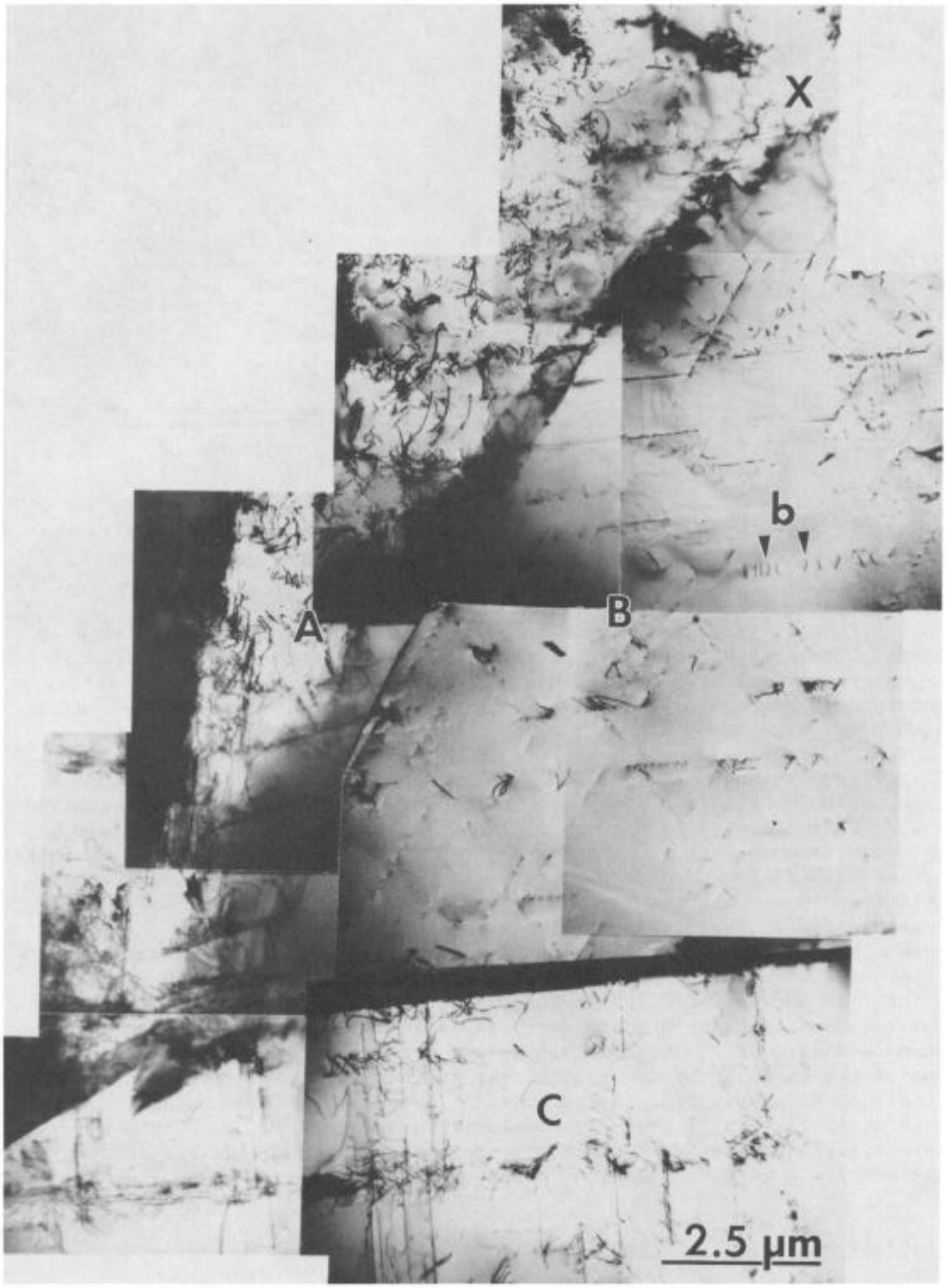

(a)

Figure 14 - (a) Predominantly unrecrystallized and (b) predominantly recrystallized regions from a sample deformed to a strain of -0.25 at 1150°C. Regions labelled X were separated by about 5μm. Letter identifications indicated in text. Montages of TEM micrographs.

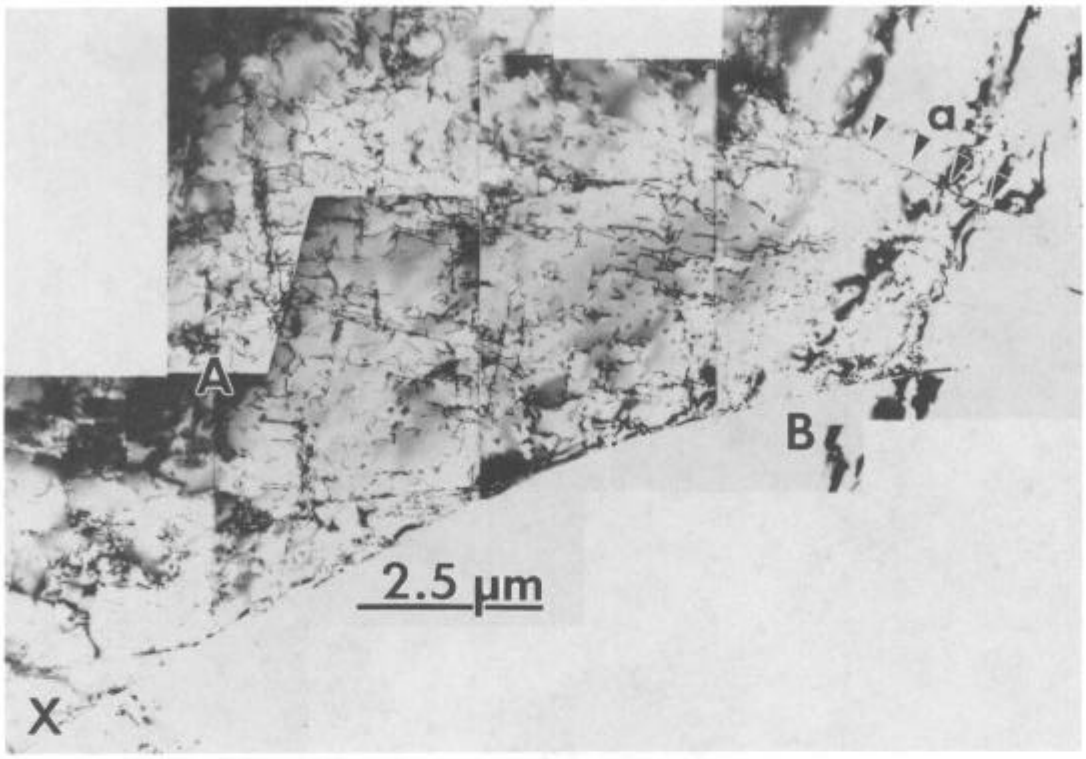

(b)

Figure 14 - (continued).

surfaces of deformed samples [15,18], dynamic recovery [20,23], precipitate cutting and disordering [24], changes in crystallographic orientation [25], and adiabatic heating [20].

To evaluate the operant softening process during deformation of as-cast alloy 718, several additional analyses were performed. The significance of adiabatic heating was determined from an analysis which included direct measurements of heating during testing and calculated strength differences due to heating [26]. For example, at a strain rate of $1.0s^{-1}$, the sample temperature increased approximately 60°C during the test. Based on an analysis of Thomas and Srinivasan [26] on the effects of strain and strain rate on temperature changes during hot compression testing, predicted isothermal stress-strain curves were obtained for each of the experimental curves shown in Figs. 2-4. As an example, Fig. 16 shows a comparison of the experimental and predicted curves for a sample deformed at 950°C at a strain rate of $1.0^{-1}s$. The curve presented in Fig. 16 represents the condition (i.e. highest strain rate and lowest temperature) where the contribution of adiabatic heating to the observed deformation behavior should be the greatest. The temperature compensated flow curve is higher than the experimental curve but still exhibits significant strain softening. Therefore, it is concluded that while adiabatic heating did contribute to the observed strain softening, other softening mechanisms made significant contributions.

Precipitate cutting as a softening mechanism was considered with compression tests of solutionized or solutionized and aged samples. Figure 17 presents the stress-strain curves for samples deformed both below (at 850°C) and above (at 950°C) the γ' solvus. The precipitates

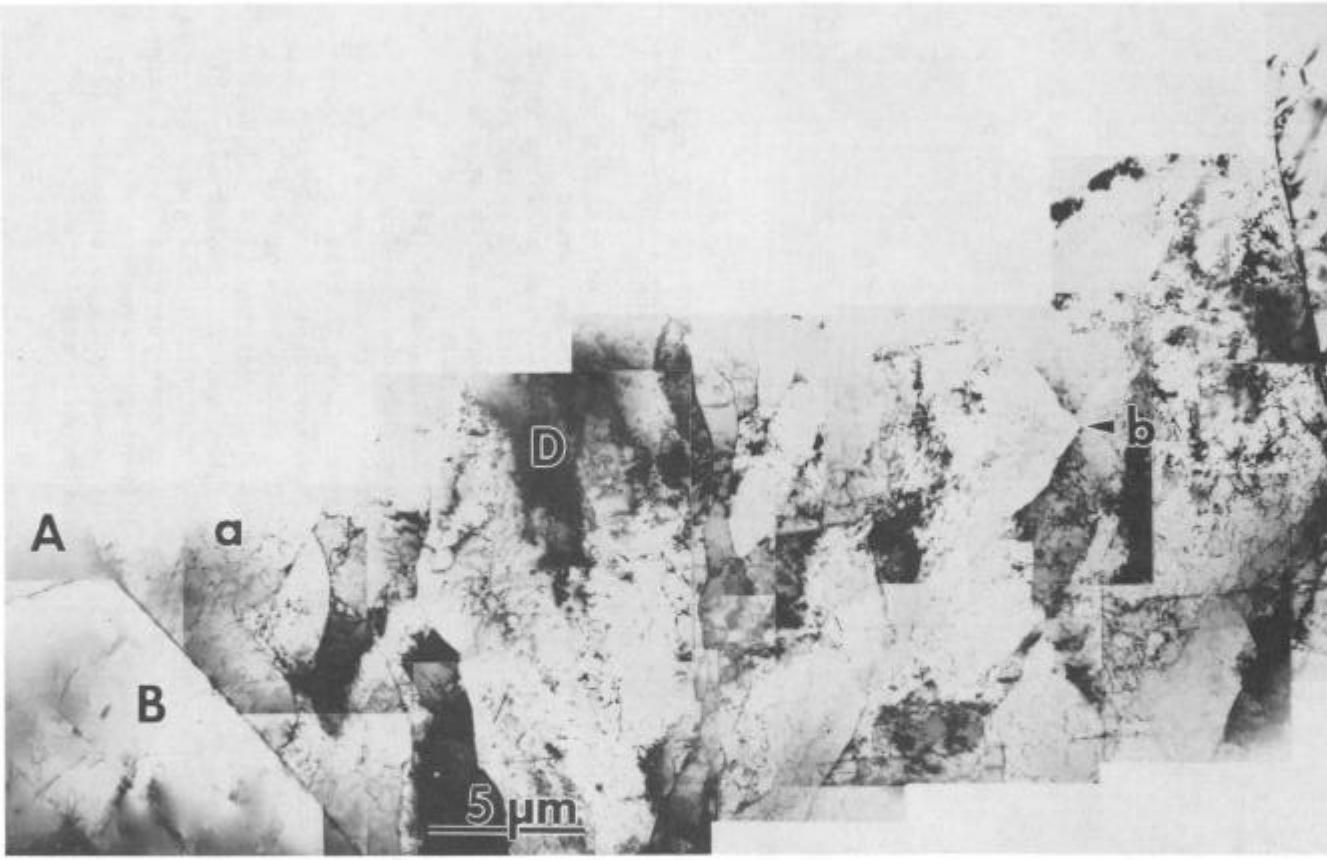

Figure 15 - Unrecrystallized region (D) surrounded by recrystallized grains (A-C) from a sample deformed to a strain of -1.0 at 1150°C.
Dislocation tangles evident at a, and sub boundary pinning apparent at b.
Montage of TEM micrographs.

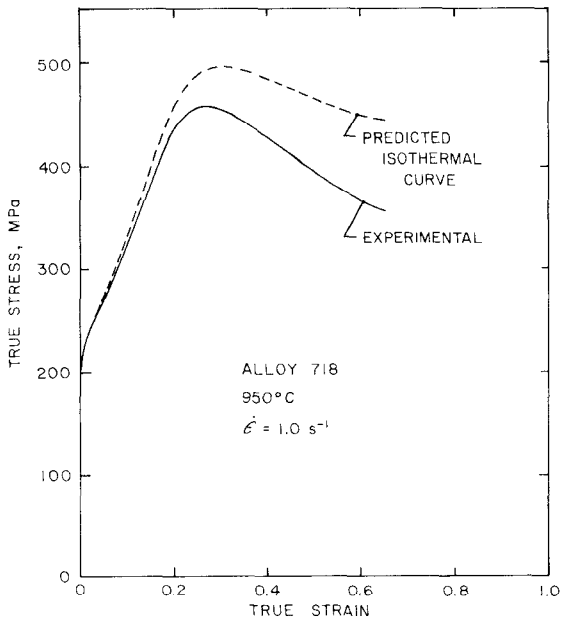

Figure 16 - A comparison of experimental and temperature compensated [26] flow curves for as-cast alloy 718 deformed at a true strain rate of 1.0 s^{-1} at 950°C.

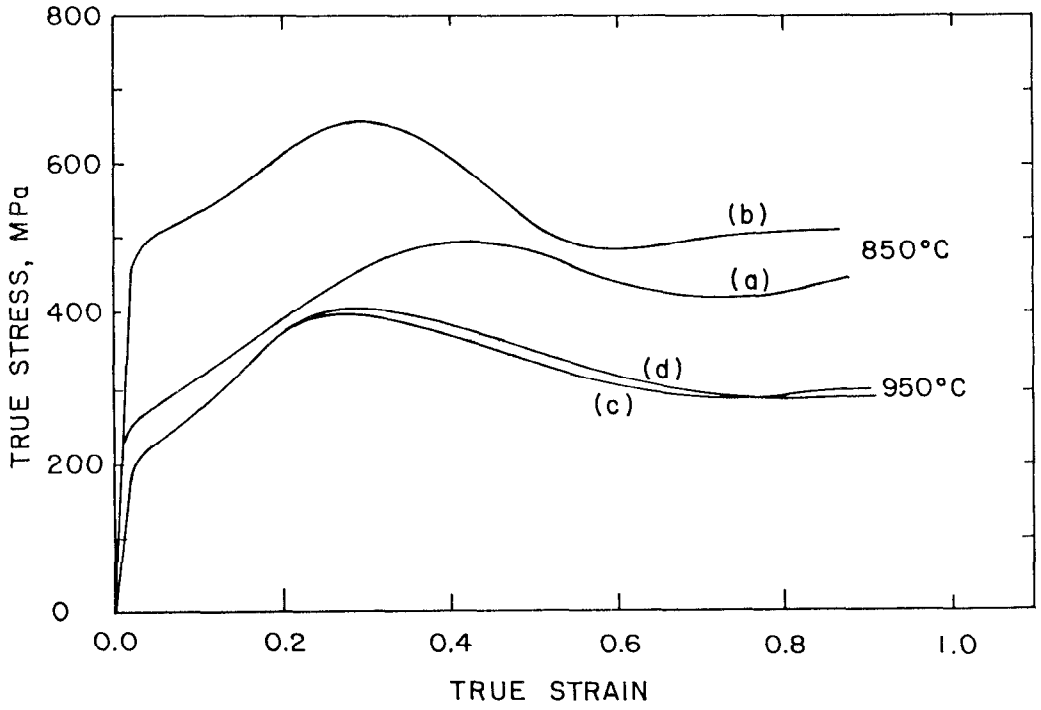

Figure 17 - True stress-true strain flow curves for samples of alloy 718 deformed at a true strain rate of 1.0 s^{-1} for two different heat treatments prior to testing. (a) solutionized, deformed at 850°C, (b) solutionized and aged, deformed at 850°C, (c) solutionized, deformed at 950°C, (d) solutionized and aged, deformed at 950°C.

present due to aging produced a significant strength increase at 850°C. However, the similarity of the stress strain curves at 950°C indicates that the precipitates dissolved during the 10 min. hold time at temperature prior to testing and thus particle cutting was not an operating softening mechanism for the tests of this study. The absence of precipitates in the tests above 950°C also provides evidence which discounts dislocation pinning by precipitates as an explanation of the yield points in alloy 718. Based on the microstructural observations, the analysis of the strain rate sensitivity data, and the indirect evidence presented in Figs. 16 and 17, it is concluded that the overall softening observed during compression testing in this study is due primarily to a combination of dynamic recovery, adiabatic heating and its effects on dynamic recovery, and shear band formation.

CONCLUSIONS

1. The hot compression stress-strain behavior of as-cast alloy 718 varied systematically with strain rate and temperature: extensive strain softening, which was observed at 950°C at the higher strain rates, decreased with a decrease in strain rate and an increase in temperature. The apparent activation energy for hot deformation of as-cast alloy 718 was 423 kJ/mole.

2. The mechanisms responsible for softening were primarily dynamic recovery, adiabatic heating and its effects on dynamic recovery, and shear band formation.

3. Recrystallization nucleated at high angle grain boundaries and primary particles. Limited dynamic recrystallization was observed. Static recrystallization, the rate of which increased with imposed strain, occurred only at test temperatures above 1050°C.

4. Based on this study, it is anticipated that hot working in the temperature range of 1050°C to 1150°C will allow uniform breakdown through large cross-sections, as a result of the strain independent flow stress at these temperatures as compared to the flow behavior at lower temperatures. Working in this range will also provide microstructural refinement as a result of static and dynamic recrystallization.

ACKNOWLEDGEMENTS

The authors acknowledge the support of the Advanced Steel Products Research Center, a National Science Foundation supported cooperative research center at the Colorado School of Mines. The authors also acknowledge the assistance of Dr. M.L. Robinson at the Carpenter Technology Corporation.

REFERENCES

1. George Krauss, ed., Deformation Processing and Structure, (Metals Park, Ohio: ASM, 1984).

2. H.J. McQueen, "The Production and Utility of Recovered Dislocation Substructures", Metall. Trans. A, 8A(1977)807-824.

3. H.J. McQueen and J.J. Jonas, Treatise on Materials Science and Technology, vol. 6, Plastic Deformation of Materials, (New York, New York: Academic Press, 1975), 393-343.

4. C.M. Sellars and W.J. McG. Tegart, "Hot Workability", Int. Met. Rev., 17(1972)1-24.

5. J.J. Jonas, C.M. Sellars, and McG. Tegart, "Strength and Structure Under Hot Working Conditions", Met. Rev., 14(1969)1-24.

6. J.L. Dillamore and W.T. Roberts, "Rolling Textures in FCC and BCC Metals", Acta Metall., 12(1964)281-293.

7. D.D. Keiser and H.L. Brown, "A Review of the Physical Metallurgy of Alloy 718", Report #ANCR-1292, Idaho National Engineering Laboratory, February 1976, pp. 1-27.

8. M.C. Chaturvedi and Ya Fang Han, "Strengthening Mechanisms in Inconel 718 Superalloy", Met. Sci. J., 17(1983)145-149.

9. T. Sakai, M.G. Akben, and J.J. Jonas, "Dynamic Recrystallization During the Transient Deformation of a Vanadium Microalloyed Steel", Acta Met., 31(4)(1983)631-642.

10. W. Roberts, H. Boden, and B. Ahlblom, "Dynamic Recrystallization Kinetics", Met. Sci. 13(1979)195-205.

11. M.R. Staker and N.J. Grant, "The Effects of Strain, Strain Rate and Temperature on Grain Refinement and Hot Workability of Type 305 Stainless Steel", Mat. Sci. and Eng., 75(1985)137-150.

12. G.T. Campbell, Jr., E.P. Abrahamson, and N.J. Grant, "The Recrystallization Behavior of an Austenitic Stainless Steel Ingot Structure Due to Hot Deformation", Metall. Trans., 5(1974)1876-1881.

13. C.P. Sullivan and M.J. Donachie, Jr., "Some Effects of Microstructure on the Mechanical Properties of Nickel-Base Superalloys", Met. Eng. Quart., 7(1967)36-45.

14. S.M. Allen, R.M. Pollouy, and R. Widmer: Advanced High-Temperature Alloys Processing and Properties, Nicholas J. Grant Symposium, (Metals Park, Ohio: ASM, 1985) 125-137.

15. M.J. Weis, "The Hot Deformation Behavior of As-Cast Alloy 718", M.S. Thesis, No. T-3382, Colorado School of Mines, Golden, Colorado, 1987.

16. M.C. Mataya, M.L. Robinson, D. Chang, M.J. Weis, G.R. Edwards, and D.K. Matlock, "Grain Refinement During Primary Breakdown of Alloy 718", 1987 Mechanical Working and Steel Processing Proceedings, (Warrendale, PA: TMS, 1987), pp. 235-247.

17. M.C. Mataya and D.K. Matlock, "Effects of Multiple Reductions on Grain Refinement During Hot Working of Alloy 718", in Alloy 718-Metallurgy and Applications, (Warrendale, PA: TMS, 1989) (Proceedings of International Symposium on Alloy 718, Pittsburgh, PA; this publication).

18. D.A.K.C. Chang, "The Influence of Ingot Heterogeneity Upon the Hot Deformation of Alloy 718", M.S. Thesis, No. T-3371, Colorado School of Mines, Golden, Colorado, 1987.

19. H.M. Miekk-oja and V.K. Lindroos, "The Formation of Dislocation Networks", Surface Science, 31(1972)422-455.

20. A.A. Guimaraes and J.J. Jonas, "Recrystallization and Aging Effects Associated with the High Temperature Deformation of Waspaloy and Inconel 718", Metall. Trans. A, 12A(1981)1655-1666.

21. M.J. Luton and C.M. Sellars, "Dynamic Recrystallization in Nickel and Nickel Iron Alloys During High Temperature Deformation", Acta Metall., 17(1969)1033-1043.

22. M.C. Mataya and M.J. Carr, "Characterization of Inhomogeneities in Complex Austenitic Stainless Steel Forgings", in Ref. 2 above, pp. 455-501.

23. R.B. Jensen and J.K. Tien, "Temperature and Strain Rate Dependence of Stress-Strain Behavior in a Nickel-Base Superalloy", Metall. Trans. A, 16A(1985)1049-1068.

24. M.C. Mataya, M.J. Carr, and G. Krauss, "The Effect of Hot Working on Structure and Strength of a Precipitation Strengthened Austenitic Stainless Steel", Metall. Trans. A, 15A(1984)347-367.

25. J.S. Murray, "Hot Working of an Al-15 Wt. Pct Cu Alloy with a Preferred Orientation", Metall. Trans. A, 6A(1975)1672-1674.

26. J.F. Thomas, Jr., and R. Srinivasan, "Constitutive Equations for High-Temperature Deformation, in Computer Simulation in Materials Science, ed. by R.J. Arsenault, J.R. Becler, Jr., and D.M. Esterling, (Metals Park, Ohio: ASM, 1988) 269-290.